Available online at www.sciencedirect.com
SCIENCE DIRECT®
Journal of Sound and Vibration 292 (2006) 824–843
JOURNAL OF SOUND AND VIBRATION
www.elsevier.com/locate/jsvi

Variability of modal behavior in terms of critical speeds of a gear pair due to manufacturing errors and shaft misalignments

N. Driot[a,*], J. Perret-Liaudet[b]

[a]*Laboratoire de Dynamique des Machines et des Structures, UMR 5006, INSA de Lyon, 69621 Villeurbanne Cedex, France*
[b]*Laboratoire de Tribologie et Dynamique des Systèmes, UMR 5513, École Centrale de Lyon, 69134 Écully Cedex, France*

Received 29 November 2004; received in revised form 4 July 2005; accepted 6 September 2005
Available online 2 December 2005

Abstract

This paper deals with the variability of the dynamic behavior induced by transmission error of a mass production gear pair. The origins of this variability are due to the manufacturing errors. The tolerances that are associated with shaft misalignment errors, gear tooth profile and lead errors, are considered as geometric independent random parameters. A procedure based on Taguchi's method is used to treat the tolerances statistically. The efficiency of this methodology is demonstrated by considering a simple dynamic model of a single spur gear pair. The predicted variations in dynamic behavior due to tolerances are verified by comparison with results obtained using Monte Carlo simulations. The analyzed parameters are firstly the static transmission error and the time-average mesh stiffness. As a consequence of the variability of the mesh stiffness, statistical variations of natural frequencies are observed for critical modes (high-energy modes). The related critical speed ranges are given too. At last, the variations of the high-energy mode shapes are also observed.

1. Introduction

Gears form a reliable and efficient way of transmitting rotational motion under loaded conditions. However, their noise characteristics are often unacceptable, especially for closed transmissions. Significant progress has been accomplished in analyzing gearbox noise mechanisms [1]. The transmission error, a concept that was first introduced by Harris [2], has been proposed to constitute one of the main sources of excitation for gearbox noise [3–7]. Under steady-state dynamic operating conditions, a gear mesh can generate dynamic mesh forces and moments that are transmitted to the housing through shafts and bearings. As a result, the vibrating surfaces of the housing radiate gearbox noise.

The transmission error depends on instantaneous tooth contact conditions and is governed by tooth surface geometry and elastic deformations of gear teeth and blanks. Many studies have focused on the selection of optimal tooth profile design and gear geometry to minimize transmission error [8–11], and hence, the noise radiated at a specific design load. Nonetheless, although such an optimal design has been identified, it is still difficult to manufacture gears having this optimal geometry. Designers must introduce tolerances around these

*Corresponding author. Tel.: +33 472 43 83 40; fax: +33 472 43 89 30.
E-mail addresses: nicolas.driot@insa-lyon.fr (N. Driot), joel.perret-liaudet@ec-lyon.fr (J. Perret-Liaudet).

0022-460X/$ - see front matter © 2005 Elsevier Ltd. All rights reserved.
doi:10.1016/j.jsv.2005.09.031

Nomenclature

$\mathbf{c}$	diagonal modal damping matrix
$\mathbf{C}$	damping matrix
$\mathbf{d}$	non-diagonal "modal" matrix related to matrix $\mathbf{D}$
$\mathbf{D}$	12×12 square matrix depending on pinion and gear geometry
$\mathbf{e}(t)$	equivalent force excitation vector associated with STE displacement excitation
f_i	ith eigenfrequency
f_{mesh}	mesh frequency
$f_{\text{rot},j}$	rotation frequency of gear j
F	input load applied on pinion
F_α, H_α	scalar parameters describing profile micro-geometry of gears
F_β, H_β	scalar parameters describing lead micro-geometry of gears
$\mathbf{g}$	vector of initial gaps related to tooth micro-geometry
$h(t)$	zero mean time counterpart of the mesh stiffness
$\mathbf{H}$	compliance matrix of contact line
$\mathbf{I}$	identity vector, $\mathbf{I}^{\mathrm{T}} = \langle 1, 1, \ldots, 1 \rangle$
$\mathbf{k}$	diagonal modal stiffness matrix
$k_m(t)$	mesh stiffness as a function of pinion angular position (or time)
$\mathbf{K}$	stiffness matrix provided by FE modeling
K_m	time-averaged value of mesh stiffness over a mesh period
$\mathbf{K}_t$	overall stiffness matrix provided by FE modeling
$\mathbf{m}$	diagonal modal mass matrix
$\mathbf{M}$	mass matrix provided by FE modeling
N_j	angular speed of gear j in rev/min
$\mathbf{p}$	pressure distribution on contact line
p_k	kth coordinate of the vector $\mathbf{p}$
$\mathbf{q}(t)$	vector of the modal coordinates
r_i	base radius of gear i
$\mathbf{s}(t)$	vector of the modal force
TB	interval of length equal to tolerance band
T_{mesh}	mesh period
$\mathbf{x}(t)$	vector of nodal displacement response
$\mathbf{y}$	vector of slack variables
y_k	kth coordinate of the vector $\mathbf{y}$
Z_j	number of teeth of gear j
Λ	static transmission error expressed as a displacement along the line of action, STE
μ, σ	respectively the mean value and standard deviation of a random variable
ρ_i	energy coefficient of the ith mode, designed for critical mode identification
θ_i	angular position of gear i ($i = 1$ pinion; 2 gear)
$\boldsymbol{\phi}_i$	ith eigenvector

nominal optimal design values. These tolerances dictate the micro- and macro-geometry of a gear and thus significantly affect transmission error and gear mesh stiffness. Robust optimization procedures were implemented in order to select optimal gear design parameters that took into account manufacturing errors and tolerances [12,13], but they mainly focused on transmission error as a response function. Even after having found an optimal design, tolerances are still responsible for variable behavior. Nonaka et al. [14] showed experimentally that noise levels radiated by mass-produced gears vary considerably. At certain rotational speeds, they reported that noise level variability can exceed 10 dB for gear pairs with the same nominal parameters. According to the authors' review, this problem had been ignored previously and a preliminary study [15] provides numerical results that correlate with the experimental results given by Nonaka et al. [14].

Precision gears are costly to manufacture and lower accuracy can lead to product failure and heavy wear. Therefore, a compromise must be found between reduced variability and cost. This compromise is especially important for automotive and industrial applications that aim at improving quality, reliability and noise characteristics without any cost penalty.

As narrowing every possible tolerance is not feasible, it is critical to identify the most sensitive parameters. This subject was dealt with by several previous studies using design of experiments and surface response functions or variance analysis. As far as gear dynamics is concerned, the parameters most sensitive to manufacturing variations were found to be profile and lead modifications applied on involute tooth geometry. The set of tolerance values on tooth geometry defines the quality class of the gear. Because it is not possible to reduce all of these tolerances, the most appropriate quality class for each characteristic has to be selected. This selection can be achieved in three steps: (1) the definition of a quality class based on the nominal values of

tooth micro-geometrical parameters; (2) the introduction of tolerances in gear dynamic modeling for computing transmission error variability as well as radiated noise level variability; and (3) the optimization of quality class choice with an objective function related to variability computed previously and cost considered as a constraint. This paper focuses on the first two steps and presents an efficient process for handling input variability and uncertainties induced by tolerances and output variability of transmission error, mesh stiffness and dynamic response of a simple gearbox. A probabilistic approach will be employed for the treatment of tolerances in the model. Statistical results will be obtained using two different methods, namely Monte Carlo simulations and Taguchi's statistical tolerancing method. A comparative study on the applicability of these methods to the gear noise problem will also be presented.

2. Dynamic modeling of a gear pair

The vibratory and acoustical behaviors of gearboxes result from numerous sources, the most common of which is static transmission error under load (STE). STE is periodic with main components at the gear mesh frequency and is basically due to (1) elastic deflections of the gear teeth under load (periodic mesh stiffness) and (2) tooth profile modifications, manufacturing errors and shaft misalignments. Under dynamic operating conditions, a gear pair excited by STE generates dynamic mesh forces that are transmitted through bearings to the housing, leading to gearbox noise. Furthermore, certain resonance conditions can exist when the gear meshing frequency is close to the natural frequencies of modes with a high level of modal potential energy stored by the mesh stiffness [16,17]. These critical natural modes are mainly controlled by the time-average mesh stiffness value.

2.1. Static transmission error computation

Static transmission error under load can be defined as the difference between the real position of the gear and that which it would have if the gear pair was geometrically perfect and rigid [6]. STE can be expressed as an angular position and, more often, as a displacement along the theoretical line of action. In order to compute STE time history, it is necessary to solve the static–elastic balance of the gear contact problem for each angular position of the pinion. Kinematic analysis of gear meshing allows locating the line of contact between teeth. The equations of the static balance generated from the discretization of theoretical contact lines in N nodes are written as

$$\mathbf{HP} = \Lambda\mathbf{I} - \mathbf{g} + \mathbf{y}, \tag{1}$$

$$\mathbf{I}^{\mathbf{T}}\mathbf{p} = F, \tag{2}$$

$$\text{either } p_k = 0 \quad \text{or} \quad y_k = 0 \tag{3}$$

subject to constraints

$$p_k \geqslant 0, \quad y_k \geqslant 0 \quad \text{and} \quad \Lambda \geqslant 0. \tag{4}$$

Here, STE is expressed as the relative gear mesh displacement along the line of action $\Lambda = r_1\theta_1 - r_2\theta_2$ where r_i is the base radius and θ_i the angular position of gear i ($i = 1, 2$). $\mathbf{p}$ and $\mathbf{y}$ are the normal load vector and the vector of slack variables respectively, both with dimension N. $\mathbf{H}$ is the non-diagonal compliance matrix of the line of contact, computed beforehand by using finite element (FE) modeling of gears [18,19]. $\mathbf{I}$ is the identity vector (all components are equal to 1) of dimension N and $\mathbf{g}$ is the vector of initial gaps that corresponds to tooth modifications and geometrical errors. Finally, F is the normal load borne by the gear teeth. Here, a modified simplex algorithm described in Refs. [20,21] is used to solve Eqs. (1)–(4).

Taking a thin-rimmed spur gear pair, whose parameters are listed in Table 1, as the reference gear pair, STE time histories shown in Fig. 1 are obtained under different static load values. Here, the teeth geometry of the two gears is modified parabolically in both profile and lead directions with amounts respectively equal to 20 and 16 μm such that $F = 3000$ N represents the design load.

Table 1
Main geometrical characteristics of the spur gear pair

	Pinion		Gear
Number of teeth	37		71
Base radius (mm)	52.153		100.077
Normal module (mm)		3	
Pressure angle		20°	
Face width (mm)		24	
Center distance (mm)		162	

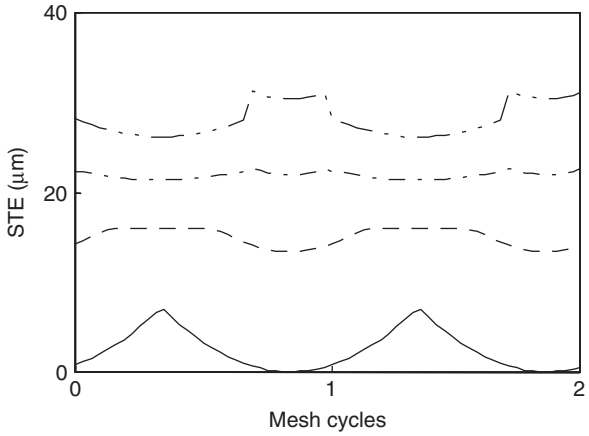

Fig. 1. STE time histories of the example gear pair at different load values: ——, 0 N; – – –, 1500 N; – · –, 3000 N; — · · —, 4500 N.

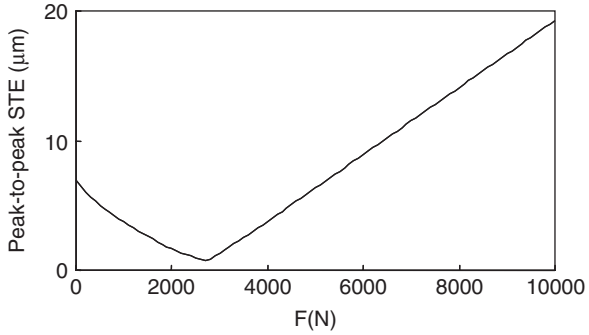

Fig. 2. Peak-to-peak value of STE versus the input load F.

In Fig. 1, STE functions are clearly periodic at the mesh period ($T_{\text{mesh}} = f_{\text{mesh}}^{-1}$) and are rather sensitive to the value of the input load applied. The first curve at $F = 0$ N corresponds to the (unloaded) STE kinematics due to only profile and lead modifications. Fig. 2 displays the peak-to-peak value of STE for the same reference spur gear versus the value of the input load, further confirming that the design load is close to 3000 N.

2.2. Mesh stiffness computation

Generally, out of plane deflections are assumed to be negligible. As a consequence, the transmitted normal load is modeled by a single spring acting on the plane of action. The related stiffness is the so-called mesh

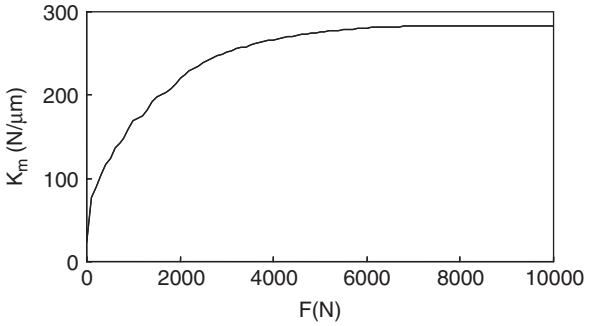

Fig. 3. Time-average value of the mesh stiffness versus input load F.

stiffness. It depends on both the static load and the angular position of the gears. For a constant operating speed, the mesh stiffness is a periodic function at the known mesh frequency. For each pinion angular position θ_1, the STE computation allows an estimation of the mesh stiffness k_m as

$$k_m(F,\theta_1) = \partial F/\partial \Lambda \tag{5}$$

or written approximately as

$$k_m \approx \delta F/[\Lambda(F+\delta F,\theta_1) - \Lambda(F,\theta_1)], \tag{6}$$

where δF is a small load increment.

The time-average value of the mesh stiffness K_m, which governs the values of all gearbox natural frequencies, is estimated by averaging $k_m(t)$ over a mesh period. For the reference gear pair concerned, Fig. 3 displays the time average of mesh stiffness K_m versus the input load. Whereas K_m varies significantly under light loads, its values tend to be relatively constant beyond the design load. This behavior is a consequence of the fact that the involute contact ratio remains relatively constant under heavier loads. For $F = 3000$ N, time average of the mesh stiffness is equal to 252 N/μm for the reference system concerned.

2.3. Gear pair dynamic model and modal analysis

There exists numerous publications about gear dynamic dealing with a large variety of models as reported for example in Refs. [7,22]. Depending on the scope of studies, models are more or less complex. Simple models having few degrees-of-freedom are commonly used for analyzing complex phenomena such as nonlinear behaviors induced by backlash [10,23]. In this case, sophisticated gear mesh interfaces are generally developed including loss of contact, damping laws and friction forces. In this field one can quote Ref. [24] in which gear mesh is modeled with a FE approach including contact mechanics model. On the contrary, global models are generally introduced when overall dynamic and noise are in the scope of the studies [16,17,25–27]. In this case, shafts, bearings and housing properties are included but a linear gear mesh interface is often retained. This choice is essentially dictated by computer time consuming.

As one of the purposes of this study is to propose a methodology for analyzing the variability of global dynamic behavior, we have retained this last kind of models. Without loss of generality, the housing is however assumed to be rigid. The reference gear pair-shaft-bearing system under study is shown in Fig. 4 and is modeled using the FE method. The pinion and the gear are modeled with concentrated masses and inertias. A specific 12×12 stiffness matrix, i.e. $k_m\,\mathbf{D}$, is introduced to couple the pinion and gear, both of them having 6 degrees of freedom (dof). This matrix is defined from the geometric characteristics of the gear pair and from the mesh stiffness previously computed [28]. The shafts are discretized using beam elements with 2 nodes and 6 dof per nodes. The base radii are equal to 45 and 85 mm for the pinion and gear shafts, respectively. The span of the bearings is equal to 75 mm for both shafts. The motor and the external loads (respective inertias are 0.05 kg m^2 and 0.026 kg m^2) are connected to the shafts by using rotary inertia and a simple torsion stiffness element (8×10^4 N m/rad for the both). A 10 $\times$ 10 stiffness matrix is introduced to model tapered bearings

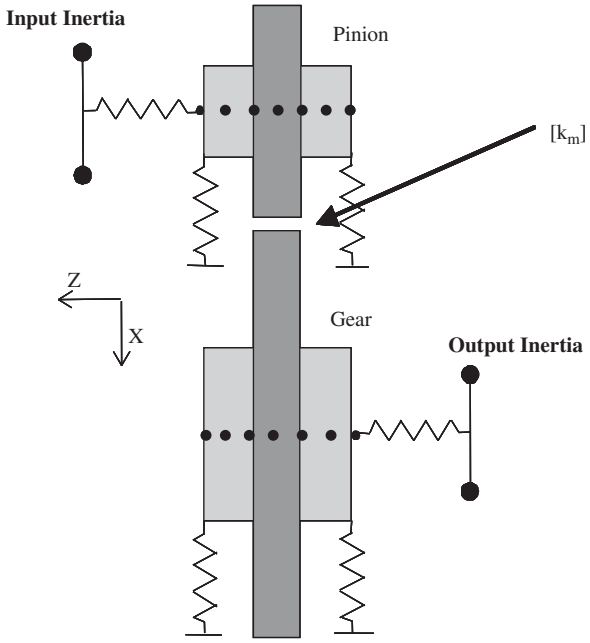

Fig. 4. Gear pair system finite element model.

with the use of the method described in Refs. [29,30]. The radial stiffnesses in the both direction are equal to 9×10^8 N/m and the axial one is equal to 1×10^8 N/m. Also, the flexural stiffnesses are equal to 5×10^4 Nm/rad. This gear pair system model contains 40 elements and a total of 200 dof.

The modal characteristics of the gear system are obtained by considering the time-average mesh stiffness K_m, and solving the corresponding eigenvalue problem. Only a few of all the natural modes are responsible for high vibratory and noise levels. These special modes, termed critical, are detected by computing an energy coefficient [16,17]. For each mode i, the energy coefficient is defined as follows:

$$\rho_i = K_m \boldsymbol{\phi}_i^{\mathrm{T}} \mathbf{D} \boldsymbol{\phi}_i / \boldsymbol{\phi}_i^{\mathrm{T}} \mathbf{K}_t \boldsymbol{\phi}_i, \tag{7}$$

where $\boldsymbol{\phi}_i$ is the ith eigenvector, K_m $\mathbf{D}$ is the stiffness matrix including only the mesh terms and $\mathbf{K}_t$ is the complete stiffness matrix of the overall system. Higher values of ρ_i indicate that this mode is more critical as it is excited by STE.

Computing the dynamic response of the gearbox requires evaluating dynamic mesh force, dynamic forces and moments transmitted to the housing through the bearings and, finally, the vibratory response of the housing. This computation needs an appropriate method. Indeed, using time integration schemes to solve the parametric matrix equation with periodic coefficients governing the forced vibrations of the gearbox has some disadvantages. Considering both low (rotation frequencies of shafts) and high frequency (mesh frequency and its harmonics) components of the excitation can increase computation time drastically, especially for systems with a large number of dof. To avoid this difficulty, a spectral and iterative method is used here [31]. This method allows the solution of a large system of differential equations with periodic coefficients within a reasonable computation time. The method is based on a spectral description of the mesh stiffness fluctuation and of the external force vector produced by STE.

The time-average mesh stiffness can be assumed to be unaffected by the dynamic motions of the gear pair for stationary running conditions when the dynamic mesh load amplitudes remain low in comparison to the static load produced by the input torque. Taking these assumptions into account, the vibratory response of the gear system is therefore governed by the following system of linear differential equations with periodic coefficients:

$$\mathbf{M}\ddot{\mathbf{x}} + \mathbf{C}\dot{\mathbf{x}} + \mathbf{K}\mathbf{x} + k_m(t)\mathbf{D}\mathbf{x} = \mathbf{e}(t). \tag{8}$$

Table 2
Natural frequencies of critical modes and corresponding energy coefficient

Modal number i	Natural frequency f_i (Hz)	Energy coefficient ρ_i (%)
1	249.9	3.6
2	407.1	2.6
6	1738.1	0.8
7	1759.8	33.7
9	2421.5	28.1
10	3666.3	0.01
11	4127.6	23.7
14	5374.2	7.2

In Eq. (8), vector $\mathbf{x}(t)$ is the vector of vibratory response of the discretized gearbox, an overdot represents differentiation with respect to time and $\mathbf{M}$ and $\mathbf{K}$ are mass and stiffness matrices provided by the FE formulation. The elastic coupling at the gear mesh is introduced by $k_m(t)$, which represents periodic mesh stiffness fluctuation and $\mathbf{D}$, a 12×12 matrix deduced from pinion and gear geometry. Matrix $\mathbf{C}$ represents the damping that is introduced later into every modal equation in the form of an equivalent viscous damping ratio for each mode. Finally, $\mathbf{e}(t)$ is an equivalent force vector associated with the displacement counterpart of STE excitation. Once the modal analysis is performed using the time-average mesh stiffness value, Eq. (8) becomes

$$\mathbf{m}\ddot{\mathbf{q}} + \mathbf{c}\dot{\mathbf{q}} + \mathbf{k}\mathbf{q} + h(t)\mathbf{d}\mathbf{q} = \mathbf{s}(t). \tag{9}$$

In Eq. (9), $\mathbf{m}$, $\mathbf{c}$ and $\mathbf{k}$ are the diagonal counterpart modal mass, damping and stiffness matrices, $\mathbf{q}(t)$ is the vector of the modal coordinates, $\mathbf{s}(t)$ is the modal force vector, $\mathbf{d}$ is a non-diagonal matrix introduced by the parametric excitation, and $h(t) = k_m(t) - K_m$ is the zero mean value mesh stiffness fluctuation. The forced response is expanded on the modal basis that has to include all critical modes. The spectral and iterative method provides the complex spectrum of the vibratory response directly for each dof of the modeled system. The processing time required by this method is about two orders of magnitude shorter than that of a classical numerical time integration scheme [31]. For memory, the fundamentals of the method are reported in appendix.

If we return to the example gear system of Fig. 4, the modal behavior is obtained by considering the average value $K_m = 252\,\mathrm{N/\mu m}$ at the input load $F = 3000\,\mathrm{N}$. Table 2 displays the natural frequencies of the most critical modes and their corresponding energy coefficients. As the sum of energy coefficients is almost equal to 100%, the range 0–5500 Hz can be seen to include all critical modes. In order to illustrate the shapes of the critical modes, Fig. 5 shows the shapes at the gear mesh for the 6, 7 and 19th modes. In relation with the energy coefficients, one can observe that the gear stiffness is not stressed for the 6th mode in contrast to the 7 and 9th modes. One can also notice that the critical modes cannot be classified as torsional or as flexural modes. Indeed, all kinds of deformations contribute to the energy storage at the gear mesh.

Once the modal data are available, the dynamic response is obtained for $K_m = 252\,\mathrm{N/\mu m}$ and STE at $F = 3000\,\mathrm{N}$, as shown in Fig. 6 in the form of dynamic mesh force amplitude versus input speed. The main resonances are observed at input speeds close to 3000 and 4000 rev/min and are due to resonant excitation of critical modes. Without any surprise, these resonances are respectively due to an excitation of the 7th and 9th modes by the mesh frequency f_{mesh}. Other secondary resonances are observed for input speeds close to 2000 and 1500 rev/min. They correspond to an excitation of the same modes by the first harmonic of STE ($2f_{\mathrm{mesh}}$).

3. Statistical description of tolerances

3.1. Description of gear tooth modifications

In this study, tolerance ranges of profile errors, lead errors and misalignments are chosen at quality class 7 of ISO 1328. This quality class is often used in industrial and automotive applications (gearboxes, machine tool, etc). Due to manufacturing errors, the real tooth surfaces deviate from the theoretical tooth surfaces. As shown schematically in Fig. 7, this gap is expressed by two parameters, H_α and F_α, which govern the profile

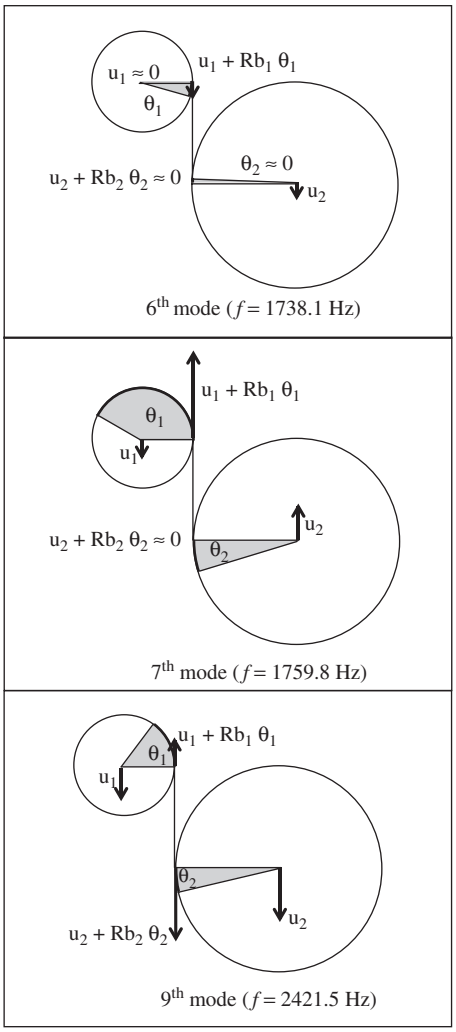

Fig. 5. Mode shapes at the gear mesh for the 6th, 7th and 9th modes ($K_m = 252\,\mathrm{N/\mu m}$).

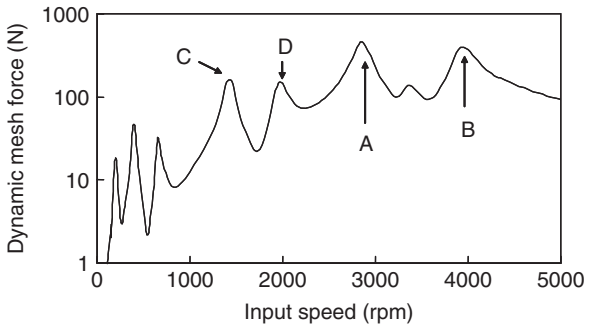

Fig. 6. Steady-state dynamic mesh force as a function of the input speed at $F = 3000\,\mathrm{N}$. Main resonances are identified as frequency of excited modes by the mesh frequency or its first harmonic (peaks A: $f_{mesh} = f_7$; B: $f_{mesh} = f_9$; C: $2f_{mesh} = f_7$; D: $2f_{mesh} = f_9$).

errors, and two additional parameters, H_β and F_β, which govern the lead errors. Here, F_α and F_β represent quadratic errors (crown) or modifications while H_α and H_β are used to describe linear errors. Manufacturing errors can be described by using these four parameters in combination. Consequently, the tooth surface shape

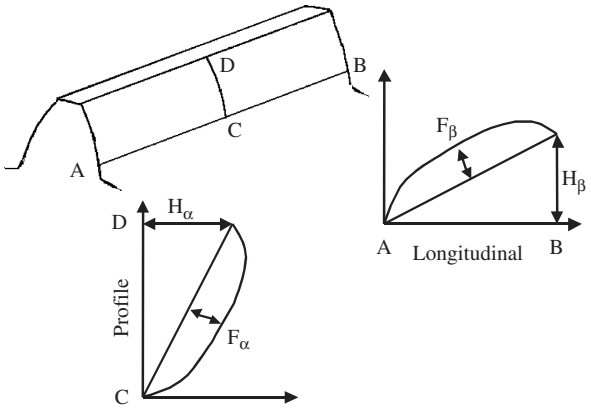

Fig. 7. Description of the manufacturing errors used.

Table 3
Statistical moments of geometry errors for an ISO 1328 Class 7 gear pair

	Mean value (μm)	Standard deviation (μm)
F_α	20	4.53
H_α	0	3.40
F_β	16	4.00
H_β	0	4.63

is approximated by a quadratic surface. In reality, this assumption covers most practical cases, even if tooth-to-tooth variability is neglected. Finally, a shaft misalignment is added through the lead H_β parameter. For the example system concerned, a design load of $F = 3000\,\mathrm{N}$ is obtained with the following intentional profile and lead modifications: $F_\alpha = 20\,\mu\mathrm{m}$, $F_\beta = 16\,\mu\mathrm{m}$ and $H_\alpha = H_\beta = 0\,\mu\mathrm{m}$.

3.2. Statistical description of manufacturing errors

In mass production, the fluctuations of design variables within their tolerance bands are considered as truncated random variables. It appears natural to use a probabilistic approach because the probability density functions (PDFs) of manufacturing errors can frequently be quantified by manufacturers. Here, the fluctuations within tolerance bands are modeled by a Gaussian variable. The mean value of such fluctuations is the nominal value of the manufacturing error (the nominal profile and lead modifications introduced previously), and its standard deviation is related to tolerance ranges and the quality class. The quality class defines a bounded interval of length equal to the tolerance band (TB), in which the manufacturing error value evolves as a Gaussian variable. The standard deviation is given by $\sigma = \mathrm{TB}/6$. This description is usually chosen in statistical robust optimization [32]. Table 3 displays mean values and standard deviations of the four parameters described previously for an ISO Class 7 gear pair. Considering the H_β parameter, the statistical independence of the lead error and the misalignment Gaussian variables is assumed. Then, the mean value and the variance of H_β parameter are obtained simply by a linear combination of lead error and misalignment statistical moments.

4. Description of statistical methods

4.1. Monte Carlo simulations

Monte Carlo simulations are commonly used to obtain reference predictions in order to test other statistical methods. Monte Carlo simulation requires a large number of samples, therefore significantly increasing

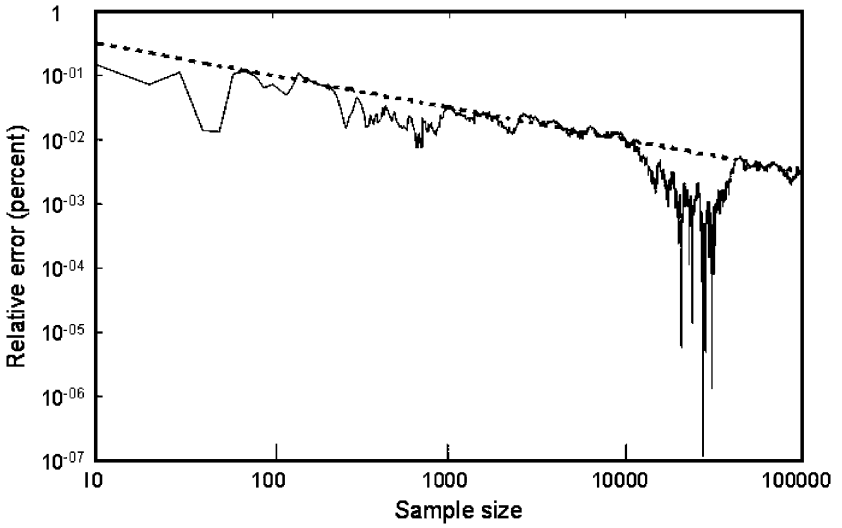

Fig. 8. Relative error in standard deviation (solid line) and function $1/\sqrt{n}$ (dotted line) versus the number of samples.

processing time since computations of STE, mesh stiffness, modal base and forced response must be performed and stored for each sample. The statistical moments and PDF are deduced at the end of the simulation. The accuracy and number of samples required greatly depend on the random number generator. In order to generate Gaussian variables, a Box and Muller algorithm is used here [33], which transforms a uniform distribution between 0 and 1 into a Gaussian one with a chosen mean value and standard deviation. The standard deviation of a Gaussian variable with a known standard deviation (equal to 1) is calculated to test the simulation process. Fig. 8 displays the relative percentage error between the estimated standard deviation and the theoretical one as a function of a number of samples n. An analytical function $1/\sqrt{n}$ is also displayed in Fig. 8. A relative error of less than 1% requires at least 10 000 samples. It can be seen that the accuracy of the Monte Carlo simulation process increases according to the $1/\sqrt{n}$ function. Consequently, the sample size chosen for future simulation is 30 000.

4.2. Taguchi's method

Taguchi's method allows estimating in a very simple way the statistical moments of a function of multiple random variables whose PDFs are known [34]. Taguchi's method has been improved by D'Errico et al. [35] for taking into account nonlinear effects as well and a modified Taguchi method has been used for heat treatment problems [36]. The theoretical expressions for the first two moments of a function $f(\mathbf{x})$ of k randomly independent variables ${}^t\mathbf{x} = \langle x_1, \ldots, x_k \rangle$ are

$$E[f(\mathbf{x})] = \int_{-\infty}^{+\infty} f(\mathbf{x}) p_1(x_1) \ldots p_k(x_k)\, \mathrm{d}x_1 \ldots \mathrm{d}x_k, \tag{10}$$

$$\mathrm{var}[f(\mathbf{x})] = \int_{-\infty}^{+\infty} (f(\mathbf{x}) - E[f(\mathbf{x})])^2 p_1(x_1) \ldots p_k(x_k)\, \mathrm{d}x_1 \ldots \mathrm{d}x_k. \tag{11}$$

In D'Errico's method, each PDF of a given random variable is sampled at three or more points and a weighting coefficient is assigned to each point depending on its PDF type. For example, Fig. 9 shows a 3-point discretization of one Gaussian variable (μ_i is the mean value and σ_i the standard deviation) with associated weightings w_i. The response function is evaluated for all point combinations, and is equivalent to a full factorial design of experiments with M responses or point combinations. The modified Taguchi process is based on numerical integration techniques such as the Gauss–Hermite quadrature method for the function of multiple variables. The mean value and the variance of the function are estimated by a linear combination of

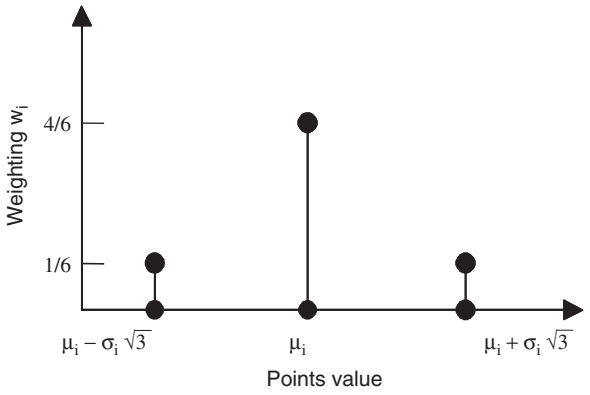

Fig. 9. Points and weightings for a Gaussian variable sampled with 3 points.

the responses obtained previously with full factorial design of experiments as follows

$$E[f(\mathbf{x})] = \sum_{i=1}^{M} W_i f_i, \tag{12}$$

$$\mathrm{var}[f(\mathbf{x})] = \sum_{i=1}^{M} W_i (f_i - E[f(\mathbf{x})])^2, \tag{13}$$

where $W_i = \prod_{i=1}^{k} w_i$. For each uncertain variable, at least three samples are necessary to take into account the nonlinear behavior of the response function. The accuracy increases rapidly with the number of samples considered. In this study, $M = 3^4 = 81$ is used to treat four random variables with 3 points per random variable. The main advantages of this method are the ease of its numerical implementation and computational efficiency. Furthermore, non-Gaussian PDFs could be easily introduced by choosing convenient points and weightings (see, for example, Ref. [37]). However, the Taguchi method cannot provide the PDF of the response function, which can be considered as a disadvantage.

5. Statistical results

5.1. Statistical variation of STE

First, the statistical variation of STE for the example system is presented. Fig. 10 presents the PDF of the peak-to-peak value of STE under four different input load levels. These PDFs are obtained by using Monte Carlo simulations. When not close to the design load ($F = 3000$ N for the example case) the PDFs take a symmetrical curve with a Gaussian shape. Close to the design load, the function of the PDF is asymmetric taking the shape of a Weibull curve. This symmetrical and asymmetrical behavior could be explained by the progression of the peak-to-peak value of STE versus the input load. Close to the design load, this progression is not a one to one mapping. For light and heavy loads, this evolution is uniform versus the input load. Table 4 compares the first two statistical moments of the peak-to-peak value of STE obtained by using both the Monte Carlo method and Taguchi's method.

All the statistical results obtained with Taguchi's method are in very good agreement with those obtained by the Monte Carlo simulations considered as the benchmark. Variability is significant since the magnitude of the standard deviation is close to the magnitude of the mean value, especially at design load $F = 3000$ N. Moreover, the peak-to-peak value of STE is not the only characteristic affected by tolerances: the STE time histories are also modified by tolerances, as shown in Fig. 11 at the design load for three possible micro-geometries within the tolerance ranges.

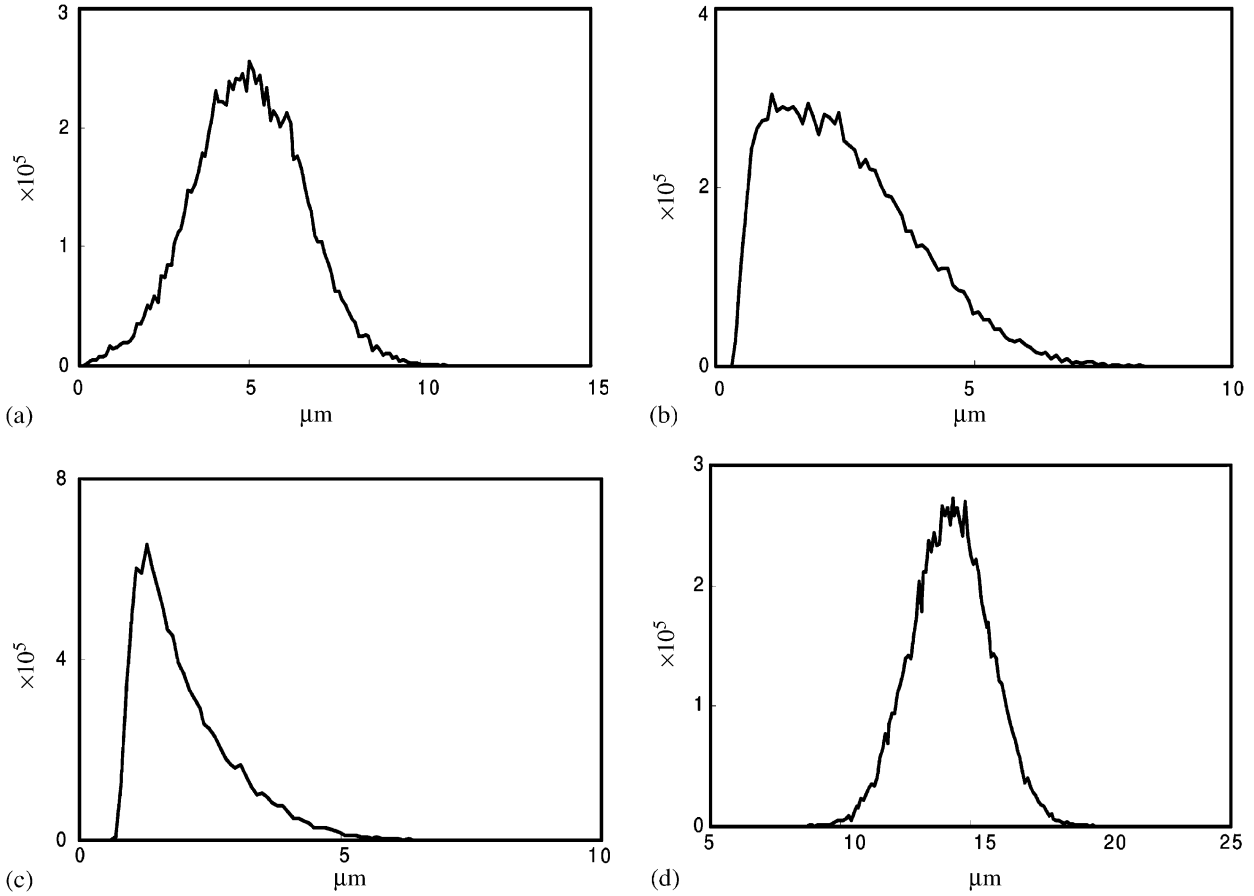

Fig. 10. PDF of the peak-to-peak value of STE at different loads: (a) $F = 500\,\mathrm{N}$, (b) $F = 1500\,\mathrm{N}$, (c) $F = 3000\,\mathrm{N}$ and (d) $F = 8000\,\mathrm{N}$.

Table 4
Mean values $E(\Lambda_{pp})$ and standard deviations $\sigma(\Lambda_{pp})$ of the peak-to-peak value Λ_{pp} of STE at different input loads

Input load F (N)	$E(\Lambda_{pp})$ Monte Carlo (μm)	$E(\Lambda_{pp})$ Taguchi (μm)	$\sigma(\Lambda_{pp})$ Monte Carlo (μm)	$\sigma(\Lambda_{pp})$ Taguchi (μm)
500	5.00	5.01	1.60	1.64
1500	2.59	2.79	1.38	1.35
3000	2.06	2.22	0.95	1.01
8000	14.3	14.3	1.52	1.52

5.2. Statistical variation of the time-averaged mesh stiffness

In Fig. 12, the PDFs of the time-average mesh stiffness obtained by Monte Carlo simulations are shown. Curves in dotted lines correspond to theoretical Gaussian functions built using the first two moments obtained by Monte Carlo simulations.

The general trend observed here is that PDFs are almost Gaussian functions regardless of F. Table 5 provides the first two statistical moments of the time-average mesh stiffness. A comparison of the variability predicted using the Monte Carlo method and Taguchi's method is listed in Table 5 for $E(K_m)$ and $\sigma(K_m)$, respectively.

The ratio of standard deviation to the mean value is within 10% for each load case. At higher loads, the mean value of the time-average mesh stiffness value is equal to the deterministic one. This is due to the fact that K_m does not change at high loads, as shown in Fig. 3 earlier.

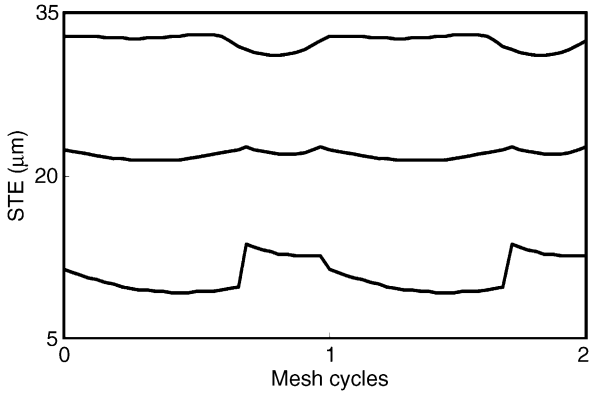

Fig. 11. Three different STE time histories at design load obtained for manufacturing errors randomly chosen within allowable tolerance bands of the ISO quality class 7.

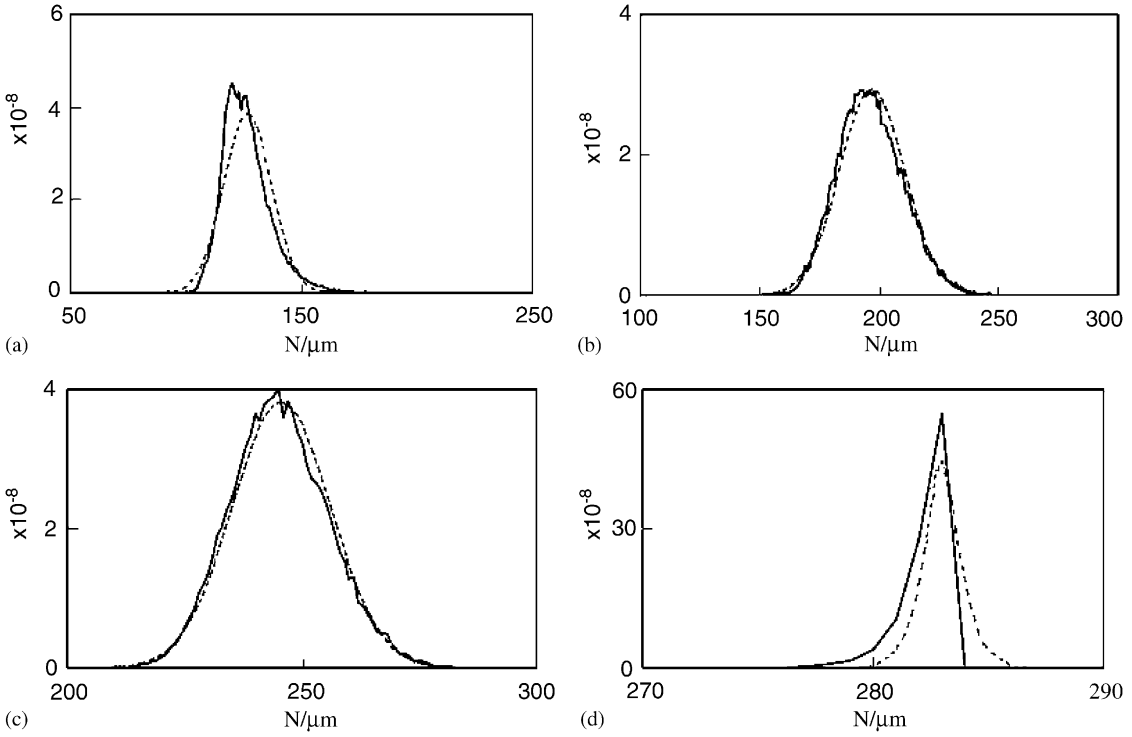

Fig. 12. PDF of K_m at different load values; (a) $F = 500\,\mathrm{N}$, (b) $F = 1500\,\mathrm{N}$, (c) $F = 3000\,\mathrm{N}$ and (d) $F = 8000\,\mathrm{N}$. Results obtained by Monte Carlo simulations (solid line) and compared to theoretical Gaussian functions (dotted line).

Table 5
Mean values $E(K_m)$ and standard deviations $\sigma(K_m)$ of K_m at different input load values

Input load F (N)	$E(K_m)$ Monte Carlo (N/μm)	$E(K_m)$ Taguchi (N/μm)	$\sigma(K_m)$ Monte Carlo (N/μm)	$\sigma(K_m)$ Taguchi (N/μm)
500	126.6	127.0	10.36	10.6
1500	197.0	197.0	13.60	12.8
3000	245.6	247.6	10.47	10.5
8000	283.0	282.0	0.89	0.95

5.3. Statistical correlation between STE and mesh stiffness

STE and K_m are physically coupled thus it seems natural that they are statistically correlated as well. Table 6 provides an estimation of the statistical correlation coefficient related to the covariance between the peak-to-peak value of STE and K_m. This coefficient is computed by using the Monte Carlo simulation.

The statistical correlation coefficient depends on the input load, but there is no obvious trend. This coefficient is negative for loads less than the design load and positive for loads higher than it. The design load corresponds to a threshold but it should be noted that statistical correlation is never equal to zero. This observation is in agreement with the progression of the peak-to-peak value of the STE versus input load shown in Fig. 2.

5.4. Influence of PDF manufacturing errors

In order to demonstrate the influence of the PDFs associated with manufacturing errors, another Monte Carlo simulation is performed which considers uniform PDFs. In this case, the first two statistical moments are summarized in Table 3 though the shape of the PDF is now uniform. Fig. 13 shows PDFs of the peak-to-peak value of STE and K_m obtained at design load $F = 3000\,\mathrm{N}$.

The PDF of the peak-to-peak value of STE is still an asymmetric function, while that of K_m is not a Gaussian one. These results confirm that there is no simple relationship between the manufacturing errors and the STE or the mesh stiffness. Knowledge of the type of PDF of the manufacturing errors is crucial because the statistical results greatly depend on their shapes.

5.5. Statistical variation of modal behavior

If we return to the example concerned and the dynamic model shown in Fig. 4, we can introduce a random time-average mesh stiffness for obtaining statistical data on the modal base. The manufacturing errors are considered here as Gaussian variables. We focus our example on design load $F = 3000\,\mathrm{N}$. Table 7 lists the first

Table 6
Statistical correlation coefficient between the STE peak-to-peak value and K_m

Input load F (N)	Correlation coefficient
500	−0.154
1500	−0.376
3000	0.233
8000	0.431

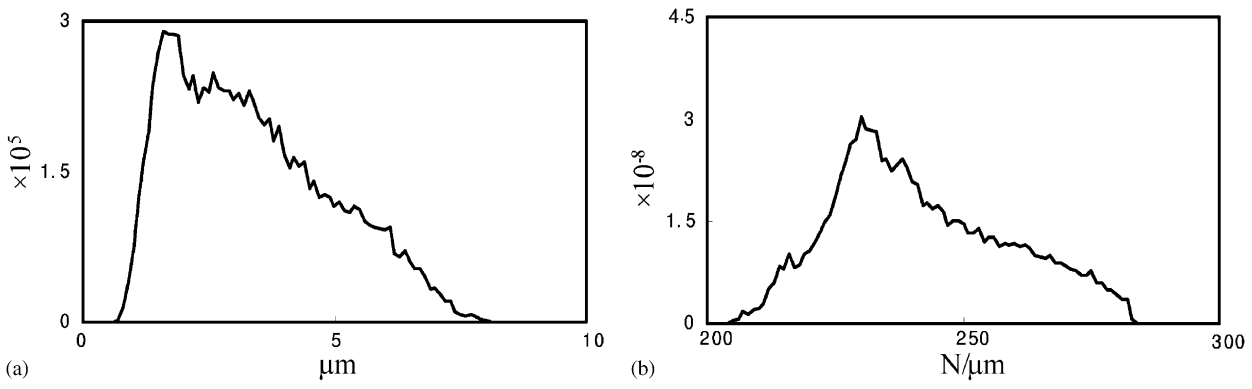

Fig. 13. PDF of the peak-to-peak value of STE (a) and time-average mesh stiffness (b) obtained at design load $F = 3000\,\mathrm{N}$.

Table 7
Mean values and standard deviations of natural frequencies and energy coefficients obtained from Monte Carlo simulations and Taguchi's method at design load $F = 3000\,\mathrm{N}$

n_i	Monte Carlo simulations				Taguchi's method			
	$E(f_i)$ (Hz)	$\sigma(f_i)$ (Hz)	$E(\rho_i)$ (%)	$\sigma(\rho_i)$ (%)	$E(f_i)$	$\sigma(f_i)$ (Hz)	$E(\rho_i)$ (%)	$\sigma(\rho_i)$ (%)
1	250	0.20	3.6	0.15	250	0.17	3.6	0.15
2	407	0.22	2.6	0.10	407	0.17	2.6	0.10
3	720	0	0	0	720	0	0	0
4	1379	0	0	0	1379	0	0	0
5	1676	0	0	0	1676	0	0	0
6	1738	0.90	2.6	3.80	1738	1.00	3.6	5.50
7	**1758**	**12.60**	**32.0**	**2.88**	**1758**	**12.60**	**31.0**	**4.30**
8	2144	0	0	0	2144	0	0	0
9	**2420**	**14.00**	**28.0**	**0.70**	**2420**	**14.00**	**28.0**	**0.70**
10	3666	0	0	0	3666	0	0	0
11	**4126**	**20.00**	**24.0**	**0.80**	**4125**	**20.00**	**23.6**	**0.90**
12	5061	0	0	0	5061	0	0	0
13	5169	0	0	0	5169	0	0	0
14	**5374**	**8.00**	**7.2**	**0.50**	**5373**	**7.80**	**7.2**	**0.50**

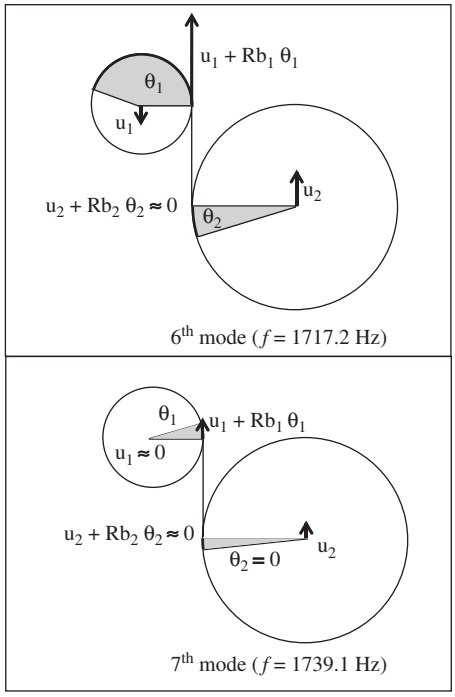

Fig. 14. Mode shapes at the gear mesh for the 6th and 7th modes for $K_m = 220\,\mathrm{N/\mu m}$.

two moments of the natural frequencies and the energy coefficients obtained for the design load, by both Monte Carlo simulations and Taguchi's method.

As one can see, the modes numbered 6 and 7 are very close, with mode number 7 being the most critical within all geometry configurations. Sometimes mode number 6 could be the most critical. That is why the standard deviation of mode number 6 is higher than its mean value. Actually, this high standard deviation exhibits an energy transfer between the two neighboring modes. This energy transfer is possible because these two modes have a non-zero energy coefficient. To illustrate it, Fig. 14 (which can be compared with Fig. 5)

shows modifications of the shapes of mode number 6 and 7 observed for a time-average mesh stiffness equal to 220 N/μm. In this case, the critical modes is now the 6th mode with an energy coefficient equal to $\rho_6 = 39.3\%$ ($\rho_7 = 0.9\%$).

The variability of the critical modes is quite small though non-negligible. Furthermore, all the results obtained with Taguchi's method are once again in very good agreement with those obtained with the Monte Carlo simulations except when an energy transfer occurs.

5.6. Critical speed ranges

The critical speeds represent the resonances when the critical natural frequencies equal the mesh frequency or its nth harmonic:

$$nZ_j f_{\mathrm{rot},j} = f_i, \tag{14}$$

where j represents the wheel (1-pinion or 2-gear), Z_j its number of teeth, $f_{\mathrm{rot},j}$ its rotation frequency and f_i represents the critical mode i and its frequency. Consequently, a critical speed N_j is expressed in rev/min as

$$N_j = 60 f_i / nZ_j. \tag{15}$$

Within an input speed range of 0 to 5000 rev/min, the critical speed bands are obtained by applying Tchebycheff's inequality and illustrated in Fig. 15. According to Tchebycheff, the critical input speed has a minimum probability of being inside range equal to 96% for each manufactured gearbox. These critical speeds correspond to a resonant excitation of the 7th and 10th modes by the mesh frequency ($n = 1$) and at its first harmonic ($n = 2$). The bandwidths are about, 200 rev/min for the 7th and 9th modes.

6. Conclusion

This study focuses on the variability of the dynamic behavior of a gear pair system caused by manufacturing errors. The selected manufacturing errors, introduced thanks to knowledge of the associated tolerances, are related to lead and profile deviations from the perfect involute flank of gear teeth and shaft misalignments are also included. We focused our attention on the static transmission error under load, the mesh stiffness and particularly its time-average value, and the modal properties of the gear pair system, i.e. all data playing a major role in gear dynamics. Concerning modal properties, only the eigenfrequencies and the energy stored at the gear mesh interface are analyzed. Consequently, the critical speeds of the gearbox, for which high dynamic tooth load and high vibratory and acoustic responses could be observed, have also been investigated. The variability of these quantities is successfully obtained, firstly by using the classical Monte Carlo simulations and, secondly, by an original approach based on a modified Taguchi method. With respect to implementation

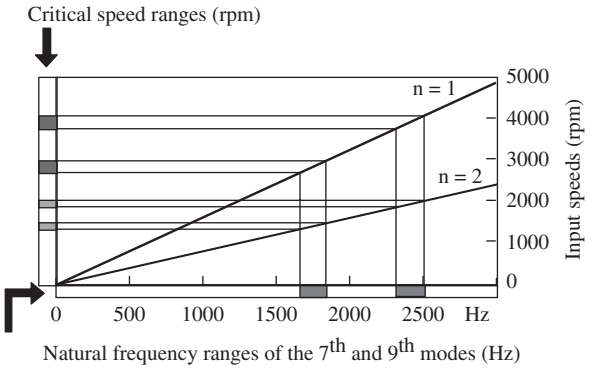

Fig. 15. The two main critical input speeds for resonant excitations of the main critical modes at mesh frequency ($n = 1$) and its first harmonic ($n = 2$).

and processing time, the latter appears to be very efficient although it does not provide the probability density functions of the responses.

Now, it is possible to conclude the following concerning all the statistical data obtained with tolerances currently used in the automotive industry:

1. There is no simple relationship between the probability density functions of manufacturing errors and the related probability density function of the STE peak-to-peak value. In particular, when the manufacturing errors are modeled by Gaussian variables, the PDF of the STE peak-to-peak value is rarely Gaussian.
2. The same remark stands for the time-average mesh stiffness, despite its probability density function being similar to a Gaussian one. It should also be noted that the STE and the mesh stiffness are statistically correlated.
3. The probability density functions of both peak-to-peak STE and time-average mesh stiffness strongly depend on manufacturing error distributions and input load.
4. The variability of the time-average mesh stiffness significantly affects the modal basis of the gear pair system. In particular, the critical modes, responsible for high dynamic responses when excited by STE, are most affected. Energy transfers between neighboring modes having similar frequencies are observed in the example case via the elastic potential energy coefficient.
5. Consequently, the critical speeds are also affected, leading to critical speed ranges. By using Tchebycheff's inequality, ranges up to 200 rev/min have been observed for the example case, around mean values of 3000 and 4000 rev/min.
6. Finally, high dispersion of dynamic levels can be predicted since strong variability of the STE peak-to-peak value exists. Assuming that a linear relationship exists between them, we can also conclude on the non-Gaussian behavior of these levels.

On the basis of these results, the author's ongoing works focus on several issues the first of which concerns the choice of the probability density functions of the manufacturing errors, because the central limit theorem cannot be applied for characterizing static transmission error and mesh stiffness. Secondly, the occurrence of critical speeds and the quantification of the dynamic levels must be considered separately. This is difficult to achieve when energy transfers occur between neighboring critical modes. Thirdly, using the modified Taguchi method for other dynamical systems appears feasible in terms of the accuracy and computational efficiency achieved.

Appendix. The iterative spectral method

The aim of this appendix is to report bases of the iterative spectral method described in Ref. [31]. We start description by considering Eq. (9), that is to say

$$\mathbf{m}\ddot{\mathbf{q}} + \mathbf{c}\dot{\mathbf{q}} + \mathbf{k}\mathbf{q} + h(t)\mathbf{d}\mathbf{q} = \mathbf{s}(t). \tag{A.1}$$

By normalizing the eigenvectors in such a way that the modal masses have unit values, the equation of motion simplifies to

$$\mathbf{I}\ddot{\mathbf{q}} + [2\zeta_j\omega_j]\dot{\mathbf{q}} + [\omega_j^2]\mathbf{q} + h(t)\mathbf{d}\mathbf{q} = \mathbf{s}(t), \tag{A.2}$$

where $\mathbf{I}$ is the identity matrix, brackets denote diagonal matrices, ω_j is the jth natural frequency defined from the undamped system in the absence of parametric excitation, and ζ_j is an equivalent viscous damping for the jth mode.

Matrix Eq. (A.2) can be rearranged by transferring the parametric excitation terms to the right-hand side thus

$$\mathbf{I}\ddot{\mathbf{q}} + [2\zeta_j\omega_j]\dot{\mathbf{q}} + [\omega_j^2]\mathbf{q} = \mathbf{s}(t) - h(t)\mathbf{d}\mathbf{q} \tag{A.3}$$

in such a way that the left-hand side corresponds to the uncoupled part of the equations of motion.

If we want to find a bounded steady-state response to the external forced system, the homogeneous time-varying counterpart of Eq. (A.3) must be asymptotically stable, which we will assume later. In this case the free response vanishes as time increases. Thus the Fourier transforms of both sides of Eq. (A.3) can be obtained by retaining only stationary terms, and yields

$$[-\omega^2 + 2i\zeta_j\omega_j + \omega_j^2]\tilde{\mathbf{q}}(\omega) = \tilde{\mathbf{s}}(\omega) - (\tilde{h} \otimes \mathbf{d}\tilde{\mathbf{q}})(\omega), \tag{A.4}$$

where the tilde denotes Fourier transforms of time functions and $\otimes$ denotes convolution.

By introducing the diagonal matrix $[H_j(\omega)]$ which represents the modal frequency response functions classically defined as

$$H_j(\omega) = \frac{1}{\omega_j^2 - \omega^2 + 2i\zeta_j\omega_j\omega} \tag{A.5}$$

the matrix equation expressed in the frequency domain and which governs the steady-state response of the dynamic system under combined parametric and external excitations can be changed to its final form of

$$\tilde{\mathbf{q}}(\omega) = [H_j(\omega)]\tilde{\mathbf{s}}(\omega) - [H_j(\omega)](\tilde{h} \otimes \mathbf{d}\tilde{\mathbf{q}})(\omega). \tag{A.6}$$

We propose to solve this matrix equation iteratively by using successive approximations

$$\tilde{\mathbf{q}}_{p+1}(\omega) = \tilde{\mathbf{q}}_0(\omega) - [H_j(\omega)](\tilde{h} \otimes \mathbf{d}\tilde{\mathbf{q}}_p)(\omega). \tag{A.7}$$

For the initial estimate, the approximate solution is obtained by cancelling out the parametric excitation; it then matches that of the corresponding "time-invariant" system:

$$\tilde{\mathbf{q}}_0(\omega) = [H_j(\omega)]\tilde{\mathbf{s}}(\omega). \tag{A.8}$$

In practice, Eq. (A.7) is iterated until convergence is reached. We have introduced some stop criteria. Firstly, one must impose a maximum number of iterations, beyond which divergence of the solution is assumed. Secondly, we make a convergence test on the measurement of the incremental vector. In practice, at the nth step, we calculate the relative error ε defined by

$$\varepsilon = \frac{|\sigma_n - \sigma_{n-1}|}{|\sigma_n|} \tag{A.9}$$

which is compared to a sufficiently small value previously imposed. In Eq. (A.9), σ_n denotes the root mean square value of coordinates q_n and $|\mathbf{u}|$ a norm of vector $\mathbf{u}$. Actually, this criterion is not rigorous but it appears that using this criterion was always sufficient in our numerical simulations. Thus no other convergence tests have been tried.

The iterative spectral method allows the response spectra for each degree of freedom to be computed directly. The first advantage of the proposed method is that the approximate solution can be constructed, as and when iterations progress, without previous knowledge of their spectral contents. This assumes the choice of a programming language which permits dynamic data storage. In addition, by using dynamic data we can consider only non-zero spectral components, and so work over a large bands of frequency without loss of efficiency. Also, because the convolution product is directly computed on the frequency domain, we obtain a far from negligible gain in computing time compared to other methods. Finally, more details can be found in Ref. [31] where comparative studies are presented.

References

[1] J. Sabot, P. Ducret, A. Sibe, Integrated vibroacoustic approach to compute and reduce gear transmission noise, *Proceedings of the Fourth World Congress on Gearing and Power Transmissions*, Paris, Vol. 3, 1999, pp. 2039–2052.

[2] L.S. Harris, Dynamic loads on the teeth of spur gears, *Proceedings of the Institution of Mechanical Engineers* 172 (1958) 87–112.

[3] R.W. Gregory, S.L. Harris, R.G. Munro, Dynamic behaviour of spur gears, *Proceedings of the Institution of Mechanical Engineers* 178 (1964) 207–226.

[4] H. Opitz, Noise of gears, *Philosophical Transactions of the Royal Society* 263 (1969) 369–380.

[5] G. Niemann, J. Baethge, Drehwegfelher, Zahnfederharte und Geraush bei Stirnrardern, *Zeitschrift des Vereines Deutscher Ingenieure* 112(4) (1970) 205–214, and 112(8) (1970) 495–499 (in German).
[6] D.B. Welbourn, Fundamental knowledge of gear noise—a survey, *Proceedings of Conference on Noise and Vibrations of Engines and Transmissions*, Cranfield Institute of Technology, Vol. C177/79, 1979, pp. 9–29.
[7] D. Rémond, P. Velex, J. Sabot, *Comportement Dynamique et Acoustique des Transmissions par Engrenages*, Synthèse Bibliographique, Publications du CETIM, Senlis France, 1993 (in French).
[8] M.S. Tavakoli, D.R. Houser, Optimum profile modifications for the minimization of static transmission errors of spur gears, *ASME Journal of Mechanisms, Transmissions, and Automation in Design* 108 (1986) 86–95.
[9] R.G. Munro, N. Yildirim, Some measurements of static and dynamic transmission errors of spur gears, *Proceedings of the International Gearing Conference*, Newcastle, 1994, pp. 371–376.
[10] A. Kahraman, G.W. Blakenship, Effect of involute tip relief on dynamic response of spur gear pairs, *ASME Journal of Mechanical Design* 121 (2) (1999) 313–315.
[11] K. Umezawa, H. Houjoh, S. Matsumura, S. Wang, Investigation of the dynamic behaviour of a helical gear system—dynamics of gear pairs with bias modification, *Proceedings of the Fourth World Congress on Gearing and Power Transmissions*, Paris, Vol. 3, 1999, pp. 1981–1990.
[12] S. Sundaresan, K. Ishii, D.R. Houser, A robust optimization procedure with variations on design variables and constraints, *ASME Advances Design Automation* 65 (1) (1993) 379–386.
[13] S. Sundaresan, K. Ishii, D.R. Houser, A procedure using manufacturing variance to design gears with minimum transmission error, *ASME Journal of Mechanical Design* 113 (3) (1991) 318–324.
[14] T. Nonaka, A. Kubo, S. Kato, T. Ohmori, Silent gear design for mass-produced gears with scatters in tooth form accuracy, *ASME Proceedings of the International Power Transmission and Gearing Conference*, Scottdale, USA, Vol. 2, 1992, pp. 589–595.
[15] N. Driot, E. Rigaud, J. Sabot, J. Perret-Liaudet, Allocation of gear tolerances to minimize gearbox noise variability, *Acustica united with Acta-Acustica* 87 (2001) 67–76.
[16] E. Rigaud, J. Sabot, Effect of elasticity of shafts, bearings, casing and couplings on the critical rotational speeds of a gearbox, *VDI Berichte* 1230 (1996) 833–845.
[17] E. Rigaud, J. Sabot, J. Perret-Liaudet, Effect of gearbox design parameters on the vibratory response of its housing, *Proceedings of the Fourth World Congress on Gearing and Power Transmissions*, Paris, Vol. 3, 1999, pp. 2143–2148.
[18] M.S. Prabhu, D.R. Houser, A hybrid finite element approach for analyzing the load distribution and transmission error in thin-rimmed gears, *VDI Berichte* 1230 (1996) 201–212.
[19] E. Rigaud, D. Barday, Modelling and analysis of static transmission error, effect of wheel body deformation and interactions between adjacent loaded teeth, *Proceedings of the Fourth World Congress on Gearing and Power Transmissions*, Paris, Vol. 3, 1999, pp. 1961–1972.
[20] T. Conry, A. Seireg, A mathematical programming method for design of elastic bodies in contact, *ASME Journal of Applied Mechanics* 93 (1) (1971) 387–392.
[21] T. Conry, A. Seireg, A mathematical programming technique for the evaluation of load distribution and optimal modifications for gear systems, *ASME Journal of Engineering for Industry* 95 (3) (1973) 1115–1122.
[22] H.N. Özgüven, D.R. Houser, Mathematical models used in gear dynamics—a review, *Journal of Sound and Vibration* 121 (1988) 383–411.
[23] A. Karahman, R. Singh, Interactions between time-varying mesh stiffness and clearance nonlinearity in a gear pair, *Journal of Sound and Vibration* 146 (1991) 135–156.
[24] R.G. Parker, S.M. Vijayakar, T. Imajo, Non-linear dynamic response of a spur gear pair: modelling and experimental comparisons, *Journal of Sound and Vibration* 237 (3) (2000) 435–455.
[25] N. Takatsu, M. Kato, K. Inoue, M. Ishikawa, Analysis and experiment on the vibration transmission in a single stage gearbox, *Proceedings of the JSME International Conference on Motion and Power Transmissions*, Hiroshima, 1991, pp. 104–109.
[26] P. Ducret, J. Sabot, Calcul du bruit rayonné par les carters des transmissions à engrenages: méthode et applications (Noise prediction of the housings of gearboxes: method and applications), *Acustica united with Acta Acustica* 84 (1998) 97–107 (in French).
[27] T.C. Lim, R. Singh, Vibration transmission through rolling element bearings—part III: geared rotor system studies, *Journal of Sound and Vibration* 151 (1) (1991) 31–54.
[28] J. Perret-Liaudet, Etude des Mécanismes de Transfert entre l'Erreur de Transmission et la Réponse Dynamique des Boîtes de Vitesses d'Automobile, PhD Thesis, Ecole Centrale de Lyon 92-07, 1992 (in French).
[29] J.M. De Mul, J.M. Vree, D.A. Maas, Equilibrium and associated load distribution in ball and roller bearings loaded in five degrees of freedom while neglecting friction—part I: general theory and application to ball bearings, *ASME Journal of Tribology* 111 (1) (1989) 142–148.
[30] J.M. De Mul, J.M. Vree, D.A. Maas, Equilibrium and associated load distribution in ball and roller bearings loaded in five degrees of freedom while neglecting friction—part II: application to roller bearings and experimental verification, *ASME Journal of Tribology* 111 (1) (1989) 149–155.
[31] J. Perret-Liaudet, An original method for computing the response of a parametrically excited forced system, *Journal of Sound and Vibration* 196 (2) (1996) 165–177.
[32] A. Parkinson, Robust mechanical design using engineering models, Special 50th Anniversary Design Issue, Combined Issue of the, *Journal of Mechanical Design and the Journal of Vibration and Acoustics* 117 (B) (1995) 48–54.
[33] R.Y. Rubinstein, *Simulation and the Monte Carlo Method*, Wiley, New York, 1981.
[34] G. Taguchi, Performance analysis design, *International Journal of Production Research* 16 (6) (1978) 521–530.

[35] J.R. D'Errico, N.A. Zaino, Statistical tolerancing using a modification of Taguchi's method, *Technometrics* 30 (4) (1988) 397–405.
[36] J.C. Yu, K. Ishii, Robust optimization method for systems with significant non linear effect, *ASME Advances Design Automation* 65 (1) (1993) 371–378.
[37] M. Abramowitz, I.A. Stegun, *Handbook of Mathematical Functions*, Dover Publications, New York, 1972.